Mathematical Biosciences and Engineering

http://www.aimspress.com/journal/MBE

MBE, 19(12): 14116–14141.
DOI: 10.3934/mbe.2022658
Received: 10 July 2022
Revised: 12 September 2022
Accepted: 14 September 2022
Published: 26 September 2022

Research article

Thermal boundary layer analysis of MHD nanofluids across a thin needle using non-linear thermal radiation

Ziad Khan[1], Hari Mohan Srivastava[2,3,4,5], Pshtiwan Othman Mohammed[6], Muhammad Jawad[1], Rashid Jan[1] and Kamsing Nonlaopon[7,*]

[1] Department of Mathematics, University of Swabi, Swabi 23561, Khyber Pakhtunkhwa, Pakistan
[2] Department of Mathematics and Statistics, University of Victoria, Victoria, British Columbia V8W 3R4, Canada
[3] Department of Medical Research, China Medical University Hospital, China Medical University, Taichung 40402, Taiwan
[4] Department of Mathematics and Informatics, Azerbaijan University, 71 Jeyhun Hajibeyli Street, AZ1007 Baku, Azerbaijan
[5] Section of Mathematics, International Telematic University Uninettuno, I-00186 Rome, Italy
[6] Department of Mathematics, College of Education, University of Sulaimani, Sulaimani 46001, Kurdistan Region, Iraq
[7] Department of Mathematics, Faculty of Science, Khon Kaen University, Khon Kaen 40002, Thailand

* **Correspondence:** Email: nkamsi@kku.ac.th; Tel: +66866421582.

Abstract: An analysis of steady two-dimensional boundary layer MHD (magnetohydrodynamic) nanofluid flow with nonlinear thermal radiation across a horizontally moving thin needle was performed in this study. The flow along a thin needle is considered to be laminar and viscous. The Rosseland estimate is utilized to portray the radiation heat transition under the energy condition. Titanium dioxide (TiO_2) is applied as the nanofluid and water as the base fluid. The objective of this work was to study the effects of a magnetic field, thermal radiation, variable viscosity and thermal conductivity on MHD flow toward a porous thin needle. By using a suitable similarity transformation, the nonlinear governing PDEs are turned into a set of nonlinear ODEs which are then successfully solved by means of the homotopy analysis method using Mathematica software. The comparison result for some limited cases was achieved with earlier published data. The governing parameters were fixed values throughout the study, i.e., $k_1 = 0.3$, $M = 0.6$, $F_r = 0.1$, $\delta_\mu = 0.3$, $\chi = 0.001$, $Pr = 0.7$, $Ec = 0.5$, $\theta_r = 0.1$, $\epsilon = 0.2$, $Rd = 0.4$ and $\delta_k = 0.1$. After detailed analysis of the present work, it was discovered that the nanofluid flow diminishes with growth in the porosity parameter, variable viscosity parameter and magnetic parameter, while it upsurges when the rate of inertia increases. The

thermal property enhances with the thermal conductivity parameter, radiation parameter, temperature ratio parameter and Eckert number, while it reduces with the Prandtl number and size of the needle. Moreover, skin friction of the nanofluid increases with corresponding growth in the magnetic parameter, porosity parameter and inertial parameter, while it reduces with growth in the velocity ratio parameter. The Nusselt number increases with increases in the values of the inertia parameter and Eckert number, while it decliens against a higher estimation of the Prandtl number and magnetic parameter. This study has a multiplicity of applications like petroleum products, nuclear waste disposal, magnetic cell separation, extrusion of a plastic sheet, cross-breed powered machines, grain storage, materials production, polymeric sheet, energy generation, drilling processes, continuous casting, submarines, wire coating, building design, geothermal power generations, lubrication, space equipment, biomedicine and cancer treatment.

Keywords: MHD flow; nonlinear thermal radiation; thin needle; thermal boundary layer analysis; HAM

1. Introduction

There is the transmission of heat from a solid body to a gas or liquid flow in a problem whose consideration involves the science of fluid motion. A flow of heat is layered on the physical motion of a fluid, and the two fields interact. In order to obtain the temperature distribution and the heat transfer rate, it is important to connect the equation of motion with the energy conservation equation. However, a comprehensive solution for the flow of a viscous fluid around a body involves significant mathematical difficulties for all fluid flow geometries. To overcome such difficulties, in the year 1904 the German aerodynamicist Ludwig Prandtl [1] introduced the concept of a boundary layer. The boundary layer idea fills a gap between the theories and practices that had previously existed (for one thing, it introduces the theoretical possibilities of drag). Furthermore, the boundary layer approach allowed the solution of viscous flow problems that would have been difficult to solve through the application of the Navier-Stokes equation to the entire flow field. Prandtl [1] showed that several viscous flow problems may be investigated by splitting them into two areas, one near solid boundaries and the other spanning the rest of the flow. Only in the thin region near a solid boundary (the boundary layers) is the influence of viscosity important. The influence of viscosity is insignificant in the region outside of the boundary layers and the fluid can be viewed as non-viscous.

Heat transfer analysis and Darcy-Forchheimer flow in porous media are utilized in a wide range of applications. Porous media can be naturally formed (e.g., wood, sponges, sand beds, rocks) or fabricated (e.g., wicks, insulation, catalytic pellet). Schaefer [2] provided an overview of engineered porous materials, while Shafer et al. [3] covered the chemistry and physics of porous media. Bilal et al. [4] investigated the convective Casson fluid flow with homogeneous–heterogeneous reactions in a Darcy-Forchheimer medium. The analysis of heat transfer and entropy generation in a stratified MHD (magnetohydrodynamic) Carreau nanofluid with gyrotactic microorganisms was performed by Naz et al. [5]. They also studied the thermal and species transportation of Eyring-Powell material over a rotating disk with swimming microorganisms [6]. A numerical investigation of Darcy-Forchheimer and EMHD nanofluid flow toward a porous medium was performed by Rasool et al. [7]. Flow of porous

Nomenclature

x:	coordinate measure in axial direction (m)
r:	coordinate measure in radial direction (m)
u:	velocity component along axial direction (ms^{-1})
v:	velocity component along radial direction (ms^{-1})
u_w:	velocity of the moving needle (ms^{-1})
u_∞:	velocity outside the boundary layer (ms^{-1})
u_c:	composite velocity (ms^{-1})
T:	temperature of fluid (K)
T_w:	wall temperature (K)
T_∞:	ambient temperature (K)
$K(T)$:	thermal conductivity (m^2s^{-1})
$\mu(T)$:	dynamic viscosity ($kgm^{-1}s^{-1}$)
ρ_f:	density of fluid (kgm^{-3})
C_b:	drag coefficient ($Jkg^{-1}K^{-1}$)
σ_s:	Boltzman constant ($Wm^{-2}K^{-4}$)
ρC_p:	effective heat capacitance ($Jm^{-3}K^{-1}$)
ψ:	stream function (m^2s^{-1})
υ_f:	kinematic viscosity (m^2s^{-1}
χ:	needle size
B_0:	applied magnetic field
k^*:	permeability of porous medium
k_e:	mean absorption coefficient
M:	magnetic parameter
k_1:	porosity parameter
Rd:	radiation parameter
$\hbar$:	convergence control parameter
F_r:	inertia parameter
ϵ:	velocity ratio parameter
δ_k:	thermal conductivity parameter
δ_μ:	variable viscosity parameter
Re:	Reynolds number
Ec:	Eckert number
Pr:	Prandtl number
$\mathscr{L}$:	auxiliary linear operator

media can find extensive industrial and scientific uses in numerous natural settings such as geothermal energy systems, hydrology, petroleum reservoirs, crude gas and oil productions, granular insulation, catalytic reactors, water movements in reservoirs, grain storage, fermentation processes and so on (see, for example, Das et al. [8], Dogonchi et al. [9], Ajarostagi [10] and Abdelmalek et al. [11]).

Heat transfer and boundary layer flow across a thin needle has become a topic of interest in current studies because of their significant applications in hot-wire anemometers, biomedicine, extrusion of a

plastic sheet, wire coating, continuous casting, submarines, geothermal power generation, lubrication and the cooling of electronic devices. The thin needle is considered as a body of revolution with a thickness that is less than the thickness of the boundary layer. Lee [12] initially considered the boundary layer formation adjacent to a thin needle in a viscous fluid. Chen and Smith [13] investigated the analytical solution of a steady forced convective laminar flow across a non-isothermal thin needle. Grosan and Pop [14] used the bvp4c programming in MATLAB software to investigate the forced convective flow across a thin needle in a nanofluid. The mixed convective boundary layer flow across vertically moving thin needles was explored by Wang [15] who calculated the numerical solution for assisting and opposing flow and discovered that the solution for assisting flow is unique, but the solution for opposing flow may be unique, dual or non-existent. The formation of boundary layer flow across a non-isothermal needle which moves in a parallel free stream, has been studied in the work [16] in which the Keller box approach was used to calculate the numerical solution to discover that dual solutions occur when a needle moves in the reverse direction of the free stream. The mixed convective flow of a water base and ethylene glycol nanofluid across a non-isothermal thin needle was investigated by Nayak et al. [17] by using a generalized differential quadrature approach. They discovered that the copper ethylene glycol based nanofluid shows the greatest improvement in the heat transfer rate. The effect of Lorentz forces and Darcy-Forchheimer on radiative nanofluid flow toward a slippery curved geometry was analyzed by Algehyne et al. [18]. A collection of the boundary layer flow across a thin needle with different physical effect in nanofluid can be seen in the works by Hayat et al. [19], Ahmad et al. [20], Narain and Uberoi [21], Ahmad et al. [22], Afridi et al. [23] and Sulochana et al. [24, 25].

The investigation of exchanges of thermal flow of a fluid through different objects has attracted researchers because of its essential physical applications including air flow past an aircraft and wind engineering. Moreover, thermal radiation is also used in different fields of technology, including biomedicine, space equipment, drilling processes, cancer treatment, and higher temperature procedures. Nadeem et al. [26] investigated the influence of thermal radiation on the boundary layer flow of a Jeffrey fluid across an exponential stretch surface by using the homotopy analysis method (HAM) to solve the problem analytically. The effects of chemical reactions and thermal radiation on MHD nanofluid have been investigated by Arulmozhi et al. [27]. In the presence of thermal radiation and a heat source/sink, a steady boundary layer flow of Powell-Eyring nanofluid toward a stretching sheet was numerically explored by Manvi et al. [28]. Tayebi et al. [29] performed numerical analysis for thermal natural convection as well as the entropy generation of (Al_2O_3-H_2O) nanoparticles toward a circular cylinder. Chamkha et al. [30] investigated the natural convection MHD nanofluid in a cavity with a radiation effect and shape factor of nanoparticles. Seyyedi et al. [31] examined the natural convection heat transfer and entropy generation for hexagonal cavities with a magnetic field and (Cu-H_2O) nanoliquid. Dogonchi et al. [32] studied MHD nanofluid flow in parallel disks during a suction/blowing process with radiation and viscous dissipation effects. Wakif [33] investigated a steady 2D MHD convective flow of a radiative Casson fluid toward a horizontal stretching sheet. Sandeep et al. [34] investigated the effect of nonlinear thermal radiation on MHD hybrid nanofluid flow with a heat source. Salleh et al. [35] investigated the impact of a magnetic field across a vertically moving thin needle in nanofluid. With MHD radiative nanofluid and stability analysis, the researchers in [36] examined the boundary layer flow and heat transmission rate through a traveling thin needle. Khan et al. [37] investigated magnetohydrodynamic thin film flow through a porous stretching sheet by focusing on the impact of thermal radiation and viscous dissipation. Jawad et

al. [38] discussed the analysis of hybrid nanofluid stagnation point flow over a stretching surface by focusing on melting heat transfer. Ramzan et al. [39] investigated the effect of melting heat transfer on the flow across a moving needle with a magnetic field. Kumar and Upreti [40] described the MHD nanofluid flow across a thin needle by employing the Joule heating effect. The researchers in [41] explored two-dimensional (2D) forced convective MHD nanofluid flow across a horizontally traveling thin needle with viscous dissipation and a heat source or sinks. Hamid [42] used chemical reactions and nonlinear thermal radiation to study the MHD Casson nanofluid flow along a vertically positioned thin needle. The impact of the Darcy-Forchheimer flow for visco-elastic fluid across a thin needle was explored by Raju et al. [43]. Using viscous dissipation, the researchers in [44] investigated the formation of entropy for hybrid nanofluid flow across a needle. Nazar et al. [45] explored the hybrid nanofluid flow of Au-TiO_2 nanoparticles across a thin needle in the presence of thermal radiation and magnetic field effects with duality solution and stability analysis. The rate of heat transfer on the MHD Casson nanofluid toward a thin needle embedded in a porous medium with non-linear radiation effects was explored by Akinshilo et al. [46]. The researchers in [47] studied dynamic control by applying the HAM for nonlinear shallow water wave equations. Based on the stochastic arithmetic, Noeiaghdam et al. [48] found optimal convergence control parameters in the HAM for integral equations. In another work [49], the authors combined the HAM with Laplace transform method to produce a new powerful method named the homotopy analysis transform method. They also combined the HAM with Wazwaz's regularization method to produce the homotopy regularization method for solving integral equations (see [50]).

It is well known that perturbation and asymptotic approximations of nonlinear problems are often broken down as nonlinearity becomes strong. Therefore, they are only valid for weakly nonlinear ODEs and PDEs in general. The HAM is an analytic approximation method for highly nonlinear problems; unlike perturbation techniques, the HAM is independent of any small/large physical parameters at all. Second, different from all of the other analytic techniques, the HAM provides us a convenient way to guarantee the convergence of the solution series so that it is valid even if nonlinearity becomes rather strong. Besides, based on the homotopy of topology, it provides us much freedom to choose the base functions, initial guesses and so on, so that complicated nonlinear ODEs and PDEs can often be solved in a simple way.

In summary, the HAM has the following advantages and disadvantages:

- Independent of small/large physical parameters.
- Guarantee of convergence.
- Flexibility on choice of base function and initial guess.
- Great generality.
- It can always provide analytic approximation efficiently, but it does not give an exact solution.
- More convergence control parameters might give better approximation, but it needs much more CPU time.

There are many publications dealing with heat transfer relating to nanofluid flow across a thin needle in the above-mentioned and other related literature, but there is hardly any study of 2D boundary layer MHD nanofluid flow across a horizontally moving thin needle with nonlinear thermal radiation. Therefore, the current study aims to fill this gap. The novelty of this work is the study of the effects of thermal radiation, a magnetic field, variable viscosity parameters, temperature ratio parameter and thermal conductivity parameters on the MHD boundary layer flow of a nanofluid across a porous thin

needle. To studies these effects we dissolved titanium dioxide (TiO_2) in water to make (TiO_2-H_2O) nanofluid. In the presence of viscous dissipation, the governing PDEs are described and are then transformed into a system of nonlinear ODEs by using an appropriate similarity transformation. The HAM algorithm is utilized to determine the solution of the modeled equations. To ensure that our code is proper, we conducted a comparison study with several earlier findings. The study presented here possesses step implementation in several engineering and industrial processes and is provides responses to the following questions below:

1) How does the rate of heat transfer improve with the addition of titanium dioxide (TiO_2) in the base fluid water?

2) What is the behavior of the velocity and temperature profiles against the decreasing size of the needle?

3) What is the behavior of the velocity and temperature profiles against the varying values of variable viscosity and thermal conductivity parameters, respectively?

2. Physical description and mathematical modeling

In this section, we will present our problem in both physical and mathematical forms. Initially the problem will be explained physically through a schematic diagram and then the obtained physical descriptions will be modeled mathematically. The main physical quantities of this study are discussed in the next subsection. Throughout this phenomenon, some relevant parameters will be encountered that will be defined mathematically with a physical explanation in the conclusion part of this section.

2.1. Physical description of the problem

We consider a steady 2D boundary layer MHD nanofluid flow across a thin needle with nonlinear thermal radiation. The thin needle flow is also considered to be laminar and viscous. The needle is considered to be moving horizontally with uniform velocity u_w in a uniform stream velocity u_∞ as illustrated in Figure 1. We assume that $v(x, r)$ and $u(x, r)$ are the components of the velocity along the radial and axial directions, respectively. The constant wall temperature at the thin needle surface and their corresponding ambient temperature are respectively, denoted by T_w and T_∞, where $T_\infty < T_w$. For the given flow system, the radius of a thin needle is defined by

$$r = R(x) = \sqrt{\frac{\chi \upsilon x}{u_c}}, \tag{2.1}$$

where χ represent the needle size and $u_c = u_w + u_\infty$ is the composite velocity. With a low Reynolds number assumption (see [51]), a magnetic field with magnetic intensity B_0 is applied, which eventually results in the induced magnetic field being ignored. We further assume that the size of the needle is thin as compared to the boundary layer thickness that forms over it, so that the pressure gradient of the needle is neglected, while the impact of curvature in the transverse direction cannot be ignored.

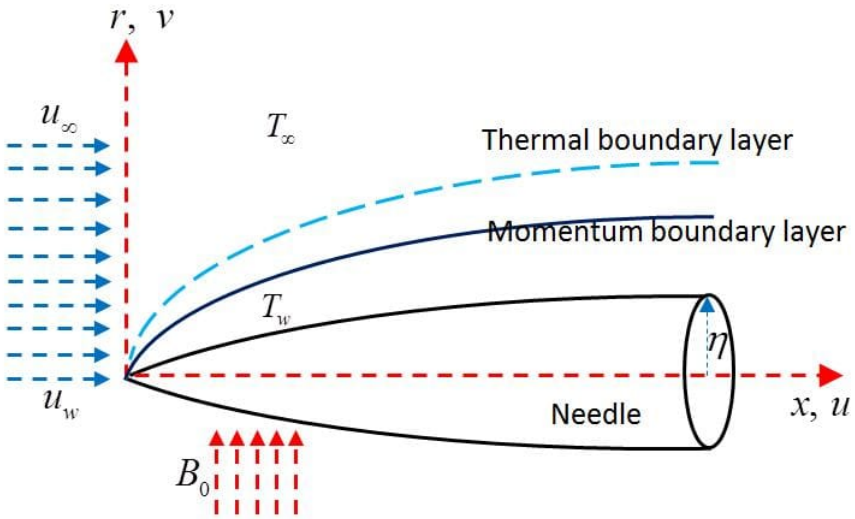

Figure 1. Geometry of the flow problem.

2.2. Mathematical modeling of the problem

Keeping in view all of the assumptions described in subsection (2.1), the governing boundary layer equation of the nanofluid flow problem transforms as follows (see [52] and [53]):

$$\frac{\partial}{\partial x}(ru) + \frac{\partial}{\partial r}(rv) = 0, \tag{2.2}$$

$$u\frac{\partial u}{\partial x} + v\frac{\partial v}{\partial r} = \frac{\mu(T)}{\rho_f}\left[\frac{1}{r}\frac{\partial u}{\partial r} + \frac{\partial^2 u}{\partial r^2}\right] + \frac{1}{\rho_f}\frac{\partial u}{\partial r}\frac{\partial \mu(T)}{\partial T} - \frac{\upsilon_f}{k^*}u - \frac{C_b}{\rho_f\sqrt{k^*}}u^2 - \frac{\sigma B_0^2}{\rho_f}u, \tag{2.3}$$

and

$$u\frac{\partial T}{\partial x} + v\frac{\partial T}{\partial r} = \frac{K(T)}{\rho C_p}\left[\frac{1}{r}\frac{\partial}{\partial r}\left(r\frac{\partial T}{\partial r}\right) - \frac{16\sigma_s T_\infty^3}{3K(T)k_e}\frac{1}{r}\frac{\partial}{\partial r}\left(r\frac{\partial T}{\partial r}\right)\right] + \frac{1}{\rho C_p}\left(\frac{\partial T}{\partial r}\right)^2\frac{\partial K(T)}{\partial T} + \frac{\mu(T)}{\rho C_p}\left(\frac{\partial u}{\partial r}\right)^2 + \frac{\sigma B_0^2}{\rho C_p}u^2, \tag{2.4}$$

subjected to the physical boundary conditions (BCs) given by

$$u = u_w, \quad v = 0, \quad T = T_w, \quad at \quad r = R(x) \quad and \quad u \to u_\infty, \quad T \to T_\infty \quad as \quad r \to \infty. \tag{2.5}$$

The thermal conductivity and kinematic viscosity of the nanofluid are respectively, denoted by $K(T)$ and $\mu(T)$ and are defined as follows (see [54]):

$$K(T) = K_0\left[1 + \delta_k\frac{T - T_\infty}{T_w - T_\infty}\right], \quad \mu(T) = \frac{\rho\upsilon_f}{1 + \delta_\mu(T - T_\infty)}. \tag{2.6}$$

In Eqs (2.2) to (2.6), the velocity components in the radial and axial directions are given, respectively, by v and u. Here ρ, u_w, C_p, T, T_w, T_∞, k^*, C_b, B_0, u_∞, δ_μ and δ_k represent the density, velocity of the moving needle, specific heat, temperature, constant surface temperature, ambient temperature, permeability of porous medium, drag coefficient, applied magnetic field, velocity outside the boundary layer, variable viscosity and thermal conductivity parameter.

To convert the model described by Eqs (2.2) to (2.4) with the BCs in Eq (2.5), we shall use the following set of similarity variables (see [55]):

$$\eta = \frac{u_c r^2}{\upsilon x}, \quad \psi = \upsilon x F(\eta), \quad \Theta = \frac{T - T_\infty}{T_w - T_\infty}. \tag{2.7}$$

After applying the Rosseland approximation, the heat flux is simplified as follows:

$$q_r = -\frac{4\sigma_s}{3k_e}\frac{\partial T^4}{\partial r}, \tag{2.8}$$

where σ_s is the Boltzman constant and k_e is the mean absorption coefficient. Expanding T_∞ by means of the Taylor series and neglecting the higher-order terms, the preceding equation can be expressed in the following form:

$$q_r = -\frac{16\sigma_s}{3k_e}T_\infty^3\frac{\partial T}{\partial r}. \tag{2.9}$$

The present study is streamlined, so ψ represents a stream function in Eq (2.7). Thus the flow characteristic component for the proposed stream function are as follows:

$$u = \frac{1}{r}\frac{\partial \psi}{\partial r}, \quad v = -\frac{1}{r}\frac{\partial \psi}{\partial x}. \tag{2.10}$$

After incorporating Eqs (2.7) and (2.10) with the relation given by Eq (2.6) into Eqs (2.2) to (2.4), we obtain the following sets of ODEs after some simplification:

$$\left[\frac{2\eta}{1+\delta_\mu\Theta}\right]F''' + \frac{1}{1+\delta_\mu\Theta}(F'' - 2\eta F''\Theta) - \frac{1}{2}(M+k_1)F' - F_rF' + \eta F'F'' + FF'' = 0, \tag{2.11}$$

$$\begin{aligned}&\frac{1+\delta_k\Theta}{Pr}\left[1 + \frac{4Rd}{3(1+\delta_k\Theta)}\left(((1+\theta_r)\Theta^3)(\eta\Theta')\right)'\right] + 2\eta\Theta'F' + 2\Theta'F + \frac{4}{Pr}(1+\delta_k\Theta)\eta\Theta'^2\\ &+16EcF''^2 + MEcF'^2 = 0.\end{aligned} \tag{2.12}$$

The dimensionless form of the subjected BCs are given by

$$\begin{aligned}&F(\eta) = \frac{\chi\epsilon}{2}, \quad \Theta(\eta) = 1, \quad F'(\eta) = \frac{\epsilon}{2} \quad at \quad \eta = \chi,\\ &F'(\eta) \to \frac{1-\epsilon}{2}, \quad \Theta(\eta) \to 0 \quad as \quad \eta \to \infty.\end{aligned} \tag{2.13}$$

It should be noticed that the parameter $\epsilon = \frac{u_w}{u_c}$ represents a significant characteristic for the flow system which is described as (a) when $\epsilon = 0$, then the needle is static and the fluid is moving; (b) when $\epsilon = 1$, then the needle is moving and the fluid is static; (c) when $0 < \epsilon < 1$, then the fluid and the needle are moving in the same directions. Furthermore, in Eqs (2.11) to (2.13) we have various emerging parameters which are present in Table 1 along with the mathematical description and physical interpretation of each of them.

2.3. Skin friction and Nusselt number

The skin friction coefficient and the local Nusselt number for our flow system are expressed as follows:

$$C_f = \frac{2\mu(T)}{\rho(u_c)^2}u_r\Big|_{r=\chi}, \quad Nu = \frac{-xT_r}{T_w - T_\infty} + q_r\Big|_{r=\chi}. \tag{2.14}$$

Using Eq (2.7) in Eq (2.14), we have these physical quantities in dimensionless form as given below (see [56]):

$$\mathrm{Re}^{\frac{1}{2}}C_f = \frac{8\sqrt{\chi}}{1+\delta_\mu}F_{\eta\eta}\Big|_{\eta=\chi}, \quad \mathrm{Re}^{-\frac{1}{2}}Nu = -2\sqrt{\chi}\left(1 + \frac{4}{3(1+\delta_k\Theta)}Rd\right)(((\theta_r - 1)\Theta)^3\,\Theta_\eta)\Big|_{\eta=\chi}. \tag{2.15}$$

Here $\mathrm{Re} = \frac{xu_c}{\upsilon_f}$ denotes the Reynolds number.

Table 1. Information of physical parameters.

Symbolic notations	Mathematical description	Physical interpretation
M	$\frac{\sigma B_0^2 x}{\rho_f u_c}$	Magnetic parameter
k_1	$\frac{\upsilon_f x}{k^* u_c}$	Porosity parameter
Rd	$\frac{4\sigma_s T_\infty^3}{k_e}$	Radiation parameter
F_r	$\frac{C_b x}{\sqrt{k^*}\rho_f u_c}$	Inertia parameter
ϵ	$\frac{u_w}{u_c}$	Velocity ratio parameter
θ_r	$\frac{T_w}{T_\infty}$	Temperature ratio parameter
δ_μ	$\delta_\mu^*(T_w - T_\infty)$	Variable viscosity parameter
Pr	$\frac{\rho C_p \upsilon_f}{K_0}$	Prandtl number
Re	$\frac{x u_c}{\upsilon_f}$	Reynolds number
Ec	$\frac{{u_c}^2}{C_p(T_w - T_\infty)}$	Eckert number

Table 2. Thermophysical properties of TiO_2 and H_2O [57].

Thermophysical properties	Titanium dioxide	water
C_p (J/kg K)	686.2	4179
K (W/mK)	8.9538	0.613
σ (S/m)	2.6×10^{6}	5.5×10^{-6}
$\beta \times 10^{-5}$(1/K)	0.9	21
ρ (kg/m^3)	4250	997.1

3. Main idea of HAM

It is well known that nonlinear ODEs and PDEs for boundary value problems are much more difficult to solve than linear ODEs and PDEs, especially by means of analytic methods. Traditionally, perturbation and asymptotic techniques are widely applied to obtain analytic approximations of nonlinear problems in science, finance and engineering. Unfortunately, perturbation and asymptotic techniques are too strongly dependent upon small/large physical parameters in general, and thus are often valid only for weakly nonlinear problems. Thus, it is necessary to develop some analytic approximation methods, which are independent of any small/large physical parameters at all and valid for strongly nonlinear problems. Therefore, in 1992, one of such kind of analytic approximation methods was proposed by the author of [58], namely the HAM.

First of all, based on the homotopy of topology, the HAM is independent of any small/large physical parameters at all. So, unlike asymptotic/perturbation techniques, the HAM can be applied to solve most nonlinear problems in science, finance and engineering, especially those without small/large physical parameters. Second, unlike all other analytical techniques, the HAM provides us a convenient way to guarantee the convergence of the solution series so that it is valid for highly nonlinear problems. Third, the HAM provides us much freedom to choose the auxiliary linear operator and base functions. Using such kind of freedom, some complicated nonlinear problems can be solved in a much easier way. Finally, the HAM logically contains the Lyapunov small artificial parameter method, Adomian decomposition method, the δ-expansion method and the Euler transform. Thus, it has great generality.

Let us first consider a nonlinear differential equation

$$\mathcal{N}[u(x,t)] = 0, \tag{3.1}$$

where $\mathcal{N}$ is a nonlinear operator, x is a vector of all spatial independent variables, t denotes the temporal independent variable and $u(x,t)$ is an unknown function, Liao [58] constructed a two-parameter family of equations in the embedding parameter $q \in[0,1]$, called the zeroth-order deformation equation

$$(1-q)\mathcal{L}[\phi(x,t;q) - u_0(x,t)] = \hbar q \mathcal{N}[\phi(x,t;q)], \tag{3.2}$$

where $\mathcal{L}$ is an auxiliary linear operator, $\hbar$ is a non-zero auxiliary parameter, $\phi(x,t;q)$ is an unknown function and $u_0(x)$ is an initial guess. At $q = 0$ and $q = 1$ we have

$$\phi(x,t;0) = u_0(x,t), \tag{3.3}$$

$$\phi(x,t;1) = u(x,t). \tag{3.4}$$

As the embedding parameter $q \in[0,1]$ increases from 0 to 1, the solution $\phi(x,t;q)$ of the zeroth-order deformation equation deforms from the initial guess $u_0(x,t)$ to the exact solution $u(x,t)$ of the original nonlinear differential equation $\mathcal{N}[u(x,t)] = 0$. Such kind of continuous variation is called deformation in topology, and this is the reason why we call Eq (3.2) the zeroth-order deformation equation. Since $\phi(x,t;q)$ is also dependent upon the embedding parameter $q \in[0,1]$, we can expand it into Maclaurin series with respect to q:

$$\phi(x,t;q) \sim u_0(x,t) + \sum_{n=1}^{\infty} u_n(x,t)q^n, \tag{3.5}$$

where

$$u_n(x,t) = \frac{1}{n!}\frac{\partial^n \phi(x,t;q)}{\partial q^n}\bigg|_{q=0}. \tag{3.6}$$

Here, Eq (3.5) is called the homotopy-Maclaurin series of $\phi(x,t;q)$. Especially, we have at $q = 1$ the homotopy series

$$\phi(x,t;1) \sim u_0(x,t) + \sum_{n=1}^{\infty} u_n(x,t). \tag{3.7}$$

If the above homotopy series is convergent to $\phi(x,t;1)$, then according to Eq (3.4), we have the homotopy series solution

$$u(x,t) = u_0(x,t) + \sum_{n=1}^{\infty} u_n(x,t), \tag{3.8}$$

which satisfies the original equation $\mathcal{N}[u(x,t)] = 0$, as proved by Liao in general. The governing equation $u_n(x,t)$ is completely determined by the zeroth-order deformation given by Eq (3.2). Differentiating Eq (3.2) n times with respect to the embedding parameter q, then dividing by $n!$ and finally setting $q = 0$, we have the so called nth-order deformation equation

$$\mathcal{L}[u_n(x,t) - \chi_n u_{n-1}(x,t)] = \hbar \mathcal{D}_{n-1}\mathcal{N}[\phi(x,t;q)], \tag{3.9}$$

where

$$\mathcal{D}_{n-1} = \frac{1}{(n-1)!}\frac{\partial^{n-1}}{\partial q^{n-1}}\bigg|_{q=0}, \tag{3.10}$$

and

$$\chi_n = \begin{cases} 0, & \text{if} \quad n \le 1 \\ 1, & \text{if} \quad n > 1. \end{cases} \tag{3.11}$$

All of these high-order deformation equations are linear with respect to the unknown $u_n(x,t)$, and thus are easy to solve by means of a computer algebra system such as Mathematica, Maple and so on.

4. HAM solution

Here, we will apply the well-known HAM for the solution of Eqs (2.11) and (2.12) with the BCs in Eq (2.13). For this aim, we utilized the Mathematica software. The basic model equation through the HAM is given below.

Linear operators in the HAM are found to be as follows:

$$\mathscr{L}_{\widehat{F}}(\widehat{F}) = \widehat{F}''', \quad \mathscr{L}_{\widehat{\Theta}}(\widehat{\Theta}) = \widehat{\Theta}'', \tag{4.1}$$

which have the subsequent applicability

$$\mathscr{L}_{\widehat{F}}(e_1\eta^2 + e_2\eta + e_3) = 0, \quad \mathscr{L}_{\widehat{\Theta}}(e_4\eta + e_5) = 0. \tag{4.2}$$

The nonlinear operators were chosen as $\mathscr{N}_{\widehat{F}}$ and $\mathscr{N}_{\widehat{\Theta}}$.

$$\begin{aligned}\mathscr{N}_{\widehat{F}}\left[\widehat{F}(\eta;q),\widehat{\Theta}(\eta;q)\right] &= \left[\tfrac{2\eta}{1+\delta_\mu\widehat{\Theta}}\right]\widehat{F}_{\eta\eta\eta} + \tfrac{1}{1+\delta_\mu\widehat{\Theta}}(\widehat{F}_{\eta\eta} - 2\eta\widehat{F}_{\eta\eta}\widehat{\Theta}) - \tfrac{1}{2}(M+k_1)\widehat{F}_\eta - F_r\widehat{F}_\eta \\ &+\eta\widehat{F}_\eta\widehat{F}_{\eta\eta} + \widehat{F}\widehat{F}_{\eta\eta},\end{aligned} \tag{4.3}$$

$$\begin{aligned}\mathscr{N}_{\widehat{\Theta}}\left[\widehat{F}(\eta;q),\widehat{\Theta}(\eta;q)\right] &= \tfrac{1+\delta_k\widehat{\Theta}}{Pr}\left[1 + \tfrac{Rd}{(1+\delta_k\widehat{\Theta})}\left(((1+\theta_r)\widehat{\Theta}^3)(\eta\widehat{\Theta}_\eta)\right)'\right] + 2\eta\widehat{\Theta}_\eta\widehat{F}_\eta + 2\widehat{\Theta}_\eta\widehat{F} \\ &+\tfrac{4}{Pr}(1+\delta_k\widehat{\Theta})\eta\widehat{\Theta}_\eta^2 + 16Ec\widehat{F}_{\eta\eta}^2 + MEc\widehat{F}_\eta^2.\end{aligned} \tag{4.4}$$

The 0^{th}-order deformation equations can be written as

$$(1-q)\mathscr{L}_{\widehat{F}}\left[\widehat{F}(\eta;q) - \widehat{F}_0(\eta)\right] = q\hbar_{\widehat{F}}\mathrm{N}_{\widehat{F}}\left[\widehat{F}(\eta;q),\widehat{\Theta}(\eta;q)\right], \tag{4.5}$$

$$(1-q)\mathscr{L}_{\widehat{\Theta}}\left[\widehat{\Theta}(\eta;q) - \widehat{\Theta}_0(\eta)\right] = q\hbar_{\widehat{\Theta}}\mathrm{N}_{\widehat{\Theta}}\left[\widehat{F}(\eta;q),\widehat{\Theta}(\eta;q)\right], \tag{4.6}$$

with the BCs given by

$$\begin{aligned}&\widehat{F}(\eta;q)\Big|_{\eta=\chi} = \tfrac{\chi\epsilon}{2}, \quad \widehat{\Theta}(\eta;q)\Big|_{\eta=\chi} = 1 \quad \tfrac{\partial\widehat{F}(\eta;q)}{\partial\eta}\Big|_{\eta=\chi} = \tfrac{\epsilon}{2}, \\ &\tfrac{\partial\widehat{F}(\eta;q)}{\partial\eta}\Big|_{\eta=\infty} = \tfrac{1-\epsilon}{2}, \quad \widehat{\Theta}(\eta;q)\Big|_{\eta=\infty} = 0.\end{aligned} \tag{4.7}$$

Here q is the embedded parameter such that $q \in [0,1]$ in order to standardize the convergence of the solutions of $\hbar_{\widehat{F}}$ and $\hbar_{\widehat{\Theta}}$. Furthermore, we chose $q = 0$ and $q = 1$ so that

$$\widehat{F}(\eta;0) = \widehat{F}_0(\eta), \quad \widehat{\Theta}(\eta;0) = \widehat{\Theta_0}(\eta), \tag{4.8}$$

$$\widehat{F}(\eta;1) = \widehat{F}(\eta), \quad \widehat{\Theta}(\eta;1) = \widehat{\Theta}(\eta). \tag{4.9}$$

Developing the Maclaurin series for $\widehat{F}(\eta;q)$ and $\widehat{\Theta}(\eta;q)$ at $q = 0$, we have

$$\widehat{F}(\eta;0) = \widehat{F}_0(\eta) + \textstyle\sum_{n=1}^{\infty}\widehat{F}_n(\eta)q^n, \tag{4.10}$$

$$\widehat{\Theta}(\eta;0) = \widehat{\Theta}_0(\eta) + \textstyle\sum_{n=1}^{\infty}\widehat{\Theta}_n(\eta)q^n, \tag{4.11}$$

where

$$\widehat{F}_n(\eta) = \tfrac{1}{n!}\tfrac{\partial^n\widehat{F}(\eta;q)}{\partial q^n}\Big|_{q=0}, \quad \widehat{\Theta}_n(\eta) = \tfrac{1}{n!}\tfrac{\partial^n\widehat{\Theta}(\eta;q)}{\partial q^n}\Big|_{q=0}. \tag{4.12}$$

The nth-order deformation equations are follows

$$\mathscr{L}_{\widehat{F}}\left[\widehat{F}_n(\eta)-\chi_n\widehat{F}_{n-1}(\eta)\right]=\hbar_{\widehat{F}}\Re_n^{\widehat{F}}(\eta), \tag{4.13}$$

$$\mathscr{L}_{\widehat{\Theta}}\left[\widehat{\Theta}_n(\eta)-\chi_n\widehat{\Theta}_{n-1}(\eta)\right]=\hbar_{\widehat{\Theta}}\Re_n^{\widehat{\Theta}}(\eta), \tag{4.14}$$

with the BCs given by

$$\widehat{F}(\eta)=\tfrac{\chi\epsilon}{2},\quad \widehat{\Theta}(\eta)=1,\quad \widehat{F}'(\eta)=\tfrac{\epsilon}{2}\quad at\quad \eta=\chi,\quad \widehat{F}'(\eta)\to\tfrac{1-\epsilon}{2},\quad \widehat{\Theta}(\eta)\to 0\quad at\quad \eta=\infty, \tag{4.15}$$

where

$$\begin{aligned}\Re_n^{\widehat{F}}(\eta)&=\left[\tfrac{2\eta}{1+\delta_\mu\widehat{\Theta}}\right]\widehat{F}'''_{n-1}+\textstyle\sum_{j=0}^{w-1}\tfrac{1}{1+\delta_\mu\Theta_{w-2-j}}(\widehat{F}''_j-2\eta\widehat{F}''_j\widehat{\Theta}_{w-1-j})-\tfrac{1}{2}(M+k_1)\widehat{F}'_{n-1}-F_r\widehat{F}'_{n-1}\\&+\eta\textstyle\sum_{j=0}^{w-1}\widehat{F}'_{w-1-j}\widehat{F}''_j+\sum_{j=0}^{w-1}\widehat{F}'_{w-1-j}\widehat{F}''_j,\end{aligned} \tag{4.16}$$

$$\begin{aligned}\Re_n^{\widehat{\Theta}}(\eta)&=\textstyle\sum_{j=0}^{w-1}\tfrac{1+\delta_k\widehat{\Theta}_{w-1-j}}{Pr}\left[1+\tfrac{Rd}{(1+\delta_k\widehat{\Theta}_{w-2-j})}\left(((1+\theta_r)\widehat{\Theta}^3_{w-3-j})(\eta\widehat{\Theta}_j)\right)'\right]+2\eta\textstyle\sum_{j=0}^{w-1}\widehat{\Theta}'_{w-1-j}\widehat{F}'_j\\&+2\textstyle\sum_{j=0}^{w-1}\widehat{\Theta}'_{w-1-j}\widehat{F}_j+\tfrac{4}{Pr}(1+\delta_k\widehat{\Theta})\eta\widehat{\Theta}^2_{n-1}+16Ec\widehat{F}^2_{n-1}+MEc\widehat{F}^2_{n-1}.\end{aligned} \tag{4.17}$$

5. Results and discussion

In this section, we discuss the graphical interpretation of a steady 2D boundary layer MHD nanofluid flow across a thin needle with nonlinear thermal radiation. The HAM algorithm has been used to find the solution of the modeled equations. All of the calculation have been made over a wide range of governing parameter values: χ = 0.2,0.1,0.01,0.001; δ_μ = 0.0,1.0,2.0,3.0; δ_k = 0.5,1.5,2.5,3.5; Ec = 1.0,2.0,3.0,4.0; ϵ = 0.0,0.3,0.6,0.9; F_r = 0.5,0.10,0.15,0.20; k_1 = 0.1,0.2,2.0,3.0; M = 0.1,0.2,0.3,0.4; Pr = 0.7,2.3,3.7,6.8; Rd = 0.4,0.6,0.8,1.0; θ_r = 1.0,1.3,1.6,1.9. In order to test the correctness of the current method, our results were compared to those obtained in earlier studies (see Ishak et al. [16] and Qasim et al. [52]) for various values of the needle size χ. Also, validation of the current code has been carried out by computing the numerical result of $\mathrm{Re}^{\frac{1}{2}}C_f$ and $\mathrm{Re}^{-\frac{1}{2}}Nu$ for different values of δ_μ and δ_k. A comparison of analytical and numerical methods exist in the literature (see [59]), therefore, we compared the HAM with the numerical method for the validity of our result. The convergence of the 0^{th}-order deformation as given by Eqs (4.5) and (4.6), wholly particular by the secondary restrictions $\hbar_F$, $\hbar_\Theta$. It is a choice in a way to control and converge the series solution. The probability of $\hbar$ is represented by $\hbar$-curves for the 25th order approximated HAM solution. The effective regions of $\hbar$ were -1.5< $\hbar_F$ <0.0 and -1.5< $\hbar_\Theta$ <0.0. The convergence of the HAM by $\hbar$-curves was used for $F''(0)$ and $\Theta'(0)$ as shown in Figures 2 and 3.

5.1. Flow characteristics

In this subsection, we discuss the effects of various physical factors such as M, k_1, F_r, δ_μ and χ upon flow characteristics as shown in Figures 4–8. From Figure 4 we observe that the fluid flow diminishes with increase in the magnetic field. Actually, applying the magnetic effect to a flow system causes the Lorentz force that opposes the flow velocity and hence, any velocity decreases would increase the magnetic parameter. Also the Lorentz force and viscous force is the ratio of hydro magnetic as suggested by M, where a higher estimation of M shows a greater Lorentz force which,

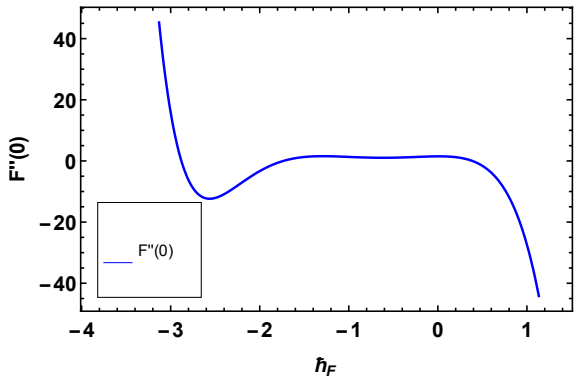

Figure 2. $\hbar_F$-curve of $F''(0)$ when $M = 0.1$, $Pr = 0.7$ and $Rd = 0.4$.

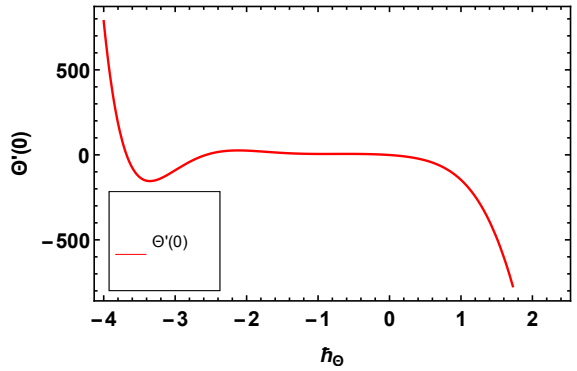

Figure 3. $\hbar_\Theta$-curve of $\Theta'(0)$ when $M = 0.1$, $Pr = 0.7$ and $Rd = 0.4$.

has the capability to slow down the flow characteristics. The variation of the porosity parameter according to the fluid properties is illustrated in Figure 5. Enhancing the porosity reduced the nanofluid velocity in the boundary layer region. It is important to note that from the appearance of an increase in the value of k_1, there was a reduction in the porous medium. Therefore, a small gap was obtained for the fluid to flow and thus we find that the flow characteristics were reduced. The nanofluid velocity for the inertia parameter is presented in Figure 6. It was discovered that, when the rate of F_r increases, the velocity function decreases. Actually, porous gaps with larger pore sizes increase viscous interference which causes a better flow resistance for greater estimation of F_r. Figure 7 illustrates the impact of a variable viscosity parameter upon the fluid properties. By increasing the value of δ_μ, the fluid becomes thicker as the resistance between the boundary layer increases; therefore, the velocity diminishes. Variation in the fluid velocity against various values of the size of the needle is displayed in Figure 8. It was observed that when the rate of χ decreases, the velocity of the fluid rises. Velocity was enhanced near the surface of the needle and decreased far away from it.

5.2. Thermal characteristics

In this subsection, we discuss the impact of Pr, Ec, θ_r, ϵ, Rd, δ_k and χ upon the thermal properties as shown in Figures 9–15. The impact of Pr on the dimensionless temperature is examined in Figure

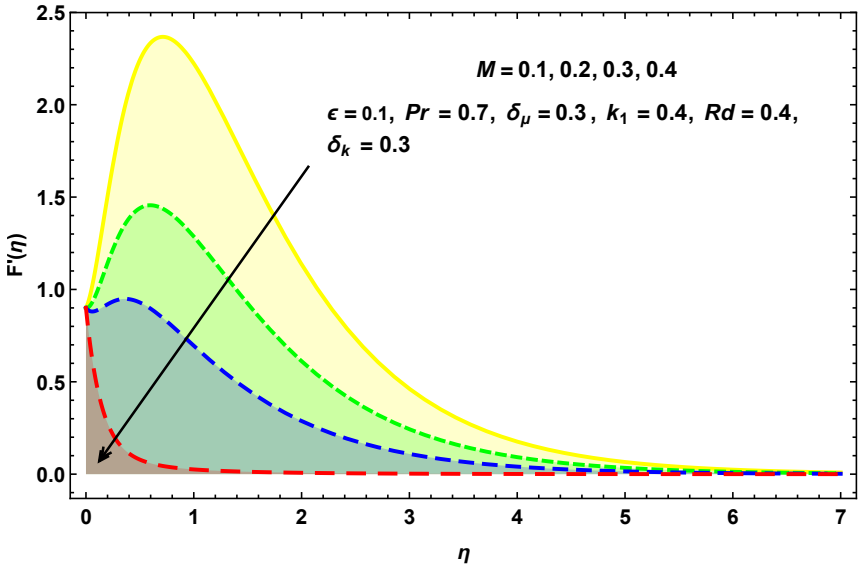

Figure 4. Variations of $F'(\eta)$ for several values of M.

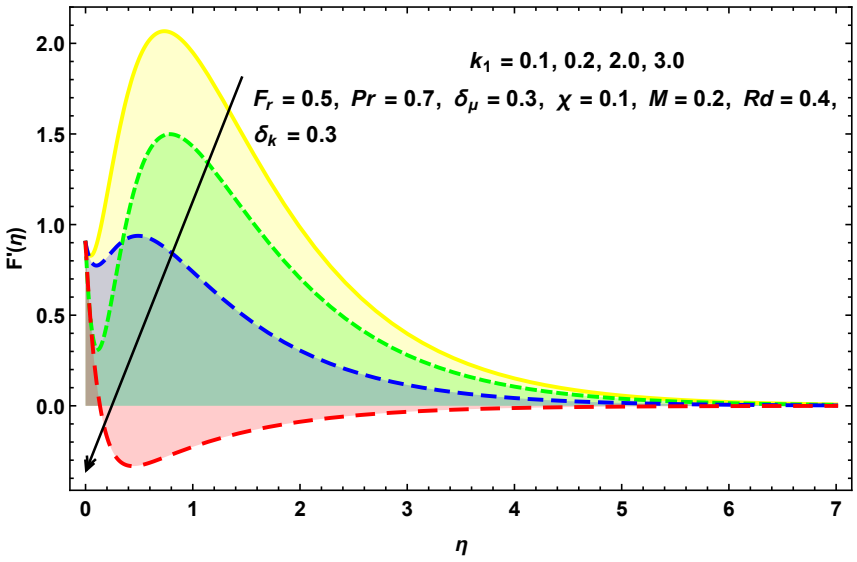

Figure 5. Variations of $F'(\eta)$ for several values of k_1.

9. The ratio of molecular diffusivity of momentum to the molecular diffusivity of heat demonstrated the relative thickness of the momentum boundary layers to the thermal boundary layers. The rises in the values of Pr decreases the fluid temperature. By enhancing the values of Pr, the thermal conductivity of the fluid diminishes and, as a result, the heat transfer rate from the needle reduces. Consequently, the thermal boundary layer and the fluid's temperature decrease. The effect of Ec on the fluid temperature is illustrated in Figure 10. The Ec parameter is a particular parameter that should be created to determine a special type of situation such that the heat enhances for larger values or reduces for smaller values. Here we have focused on the enhancing amount of Ec, and due to the dissipation heat near the thin needle surface in fast-moving flow, the thermal boundary layer thickness upsurges, which results in the temperature of the fluid increasing. The effect of θ_r on the fluid

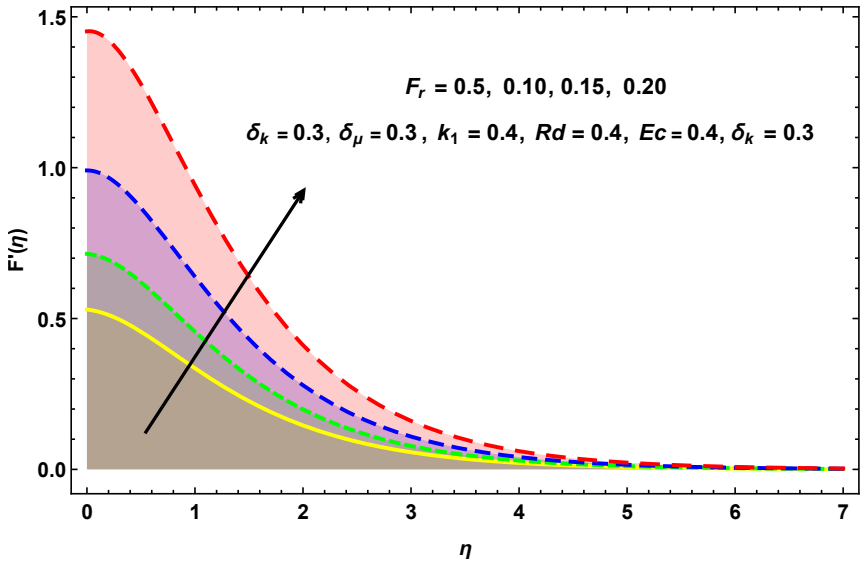

Figure 6. Variations of $F'(\eta)$ for several values of F_r.

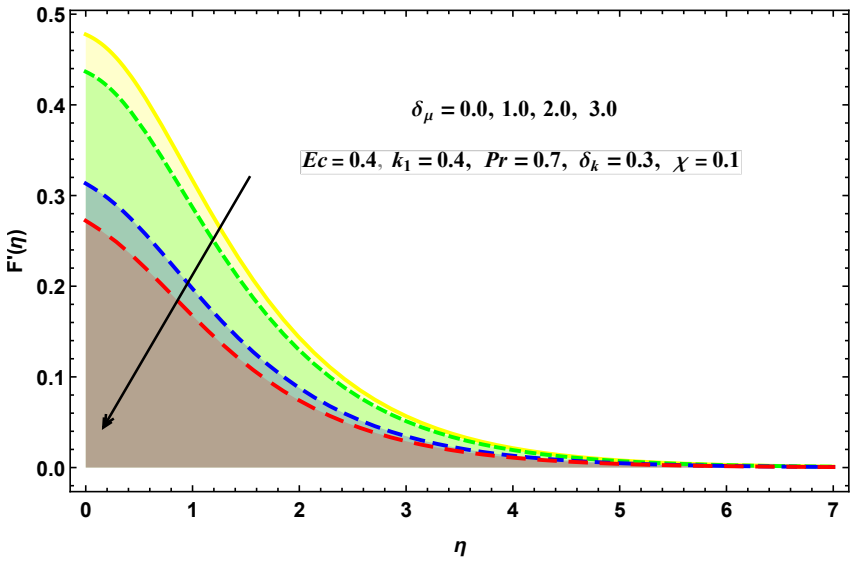

Figure 7. Variations of $F'(\eta)$ for several values of δ_μ.

temperature is illustrated in Figure 11. θ_r is the quotient of the wall temperature and the ambient temperature. Larger estimation of θ_r indicates that the wall temperature is more stable than the ambient temperature. Therefore, higher values of θ_r result in a rise in fluid temperature. Figure 12 shows that the fluid's temperature and the thermal boundary layers upsurge by enhancing the values of ϵ. The effects of Rd on the nanofluid temperature can be seen in Figure 13. In the case of high radiation, more heat is conveyed to the nanofluid. Eventually, the augmented temperature in the case of the nanofluid is witnessed. The influence of δ_k on the fluid's temperature is illustrated in Figure 14 which exhibits an enhancement in the fluid's temperature with the upsurges in the values of δ_k. It is a well-known fact that a higher thermal conductivity fluid has a higher temperature, while a lower thermal conductivity fluid has a lower temperature, that is, kinetic energy is transformed into thermal

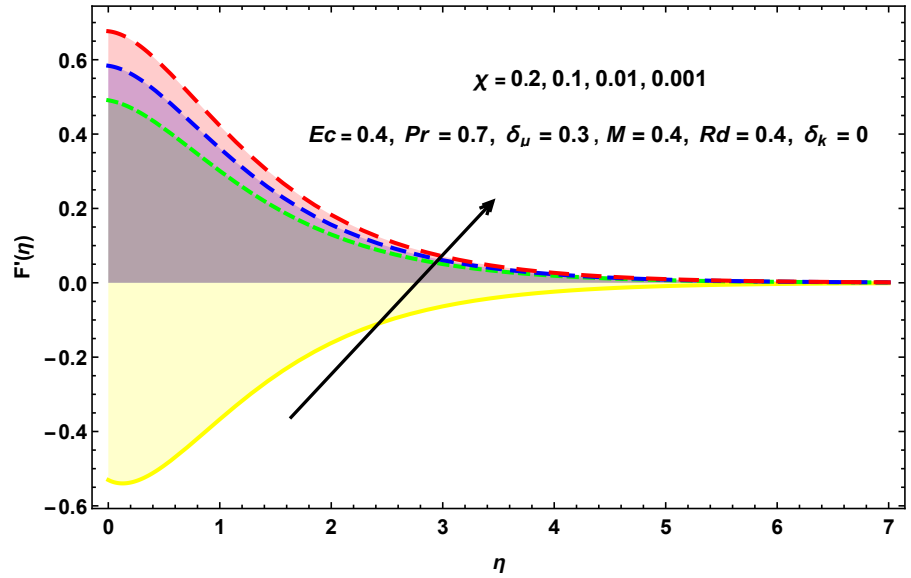

Figure 8. Variations of $F'(\eta)$ for several values of χ.

energy more rapidly; hence more heat will be lost. The influence of χ on the fluid's temperature is depicted in Figure 15. Reductions is the size of the thin needle results in the reduction of the fluid's temperature.

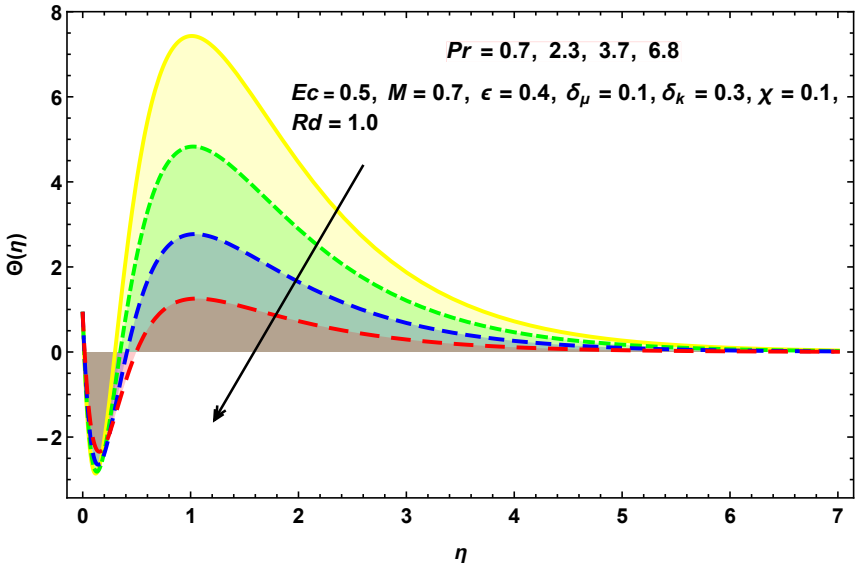

Figure 9. Variations of $\Theta(\eta)$ for several values of Pr.

5.3. Table discussion

In this subsection, we discuss the influence of different physical factors numerically upon $\mathrm{Re}^{\frac{1}{2}}C_f$ and $\mathrm{Re}^{-\frac{1}{2}}Nu$. The mathematical descriptions and physical interpretations of some physical parameters are listed in Table 1. The thermophysical properties of titanium dioxide and water are shown in Table 2. Comparisons of $F''(\eta)$, $\mathrm{Re}^{\frac{1}{2}}C_f$ and $Re^{-\frac{1}{2}}Nu$ for some values of the needle size, variable viscosity

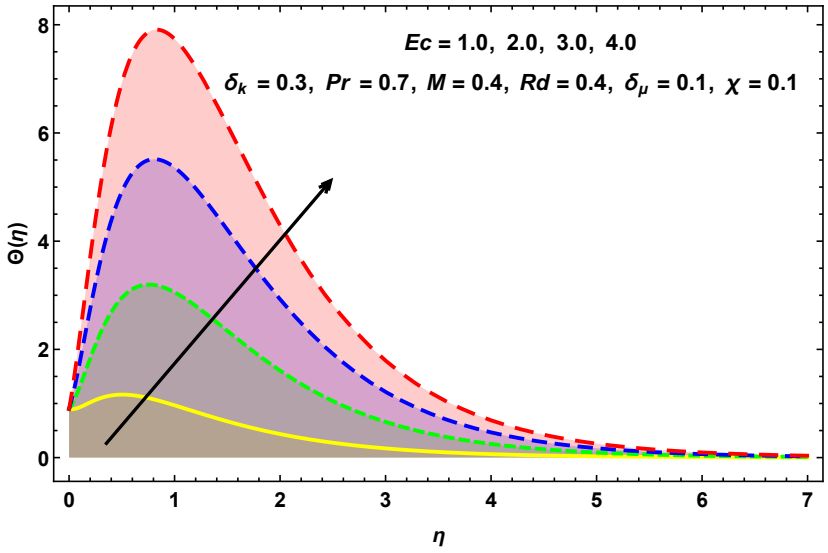

Figure 10. Variations of $\Theta(\eta)$ for several values of Ec.

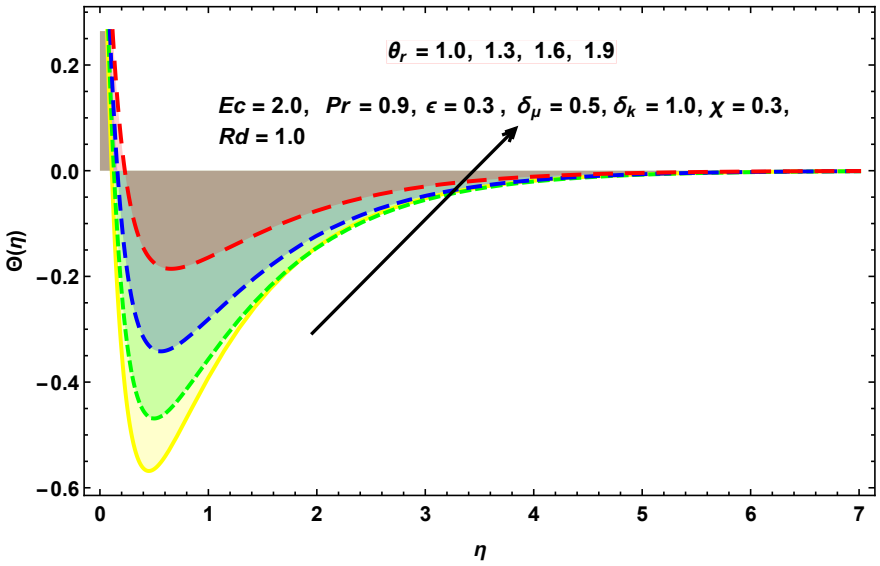

Figure 11. Variations of $\Theta(\eta)$ for several values of θ_r.

parameter and thermal conductivity parameter, respectively, are shown in Tables 3 and 4. Table 5 shows the respective influences of the velocity ratio parameter, the magnetic parameter, the porosity parameter and the inertia parameter upon skin friction numerically. For increasing values of k_1 and F_r, the skin friction is seen to enhance. Also, due to increase in the resistive force and the corresponding increase in the magnetic factor, the value of the skin friction increases. It is also revealed from this table that the skin friction reduces for upsurged values of ϵ. The variation of different physical factors on the Nusselt number is described numerically in Table 6 . The Nusselt number increases with increases in the Eckert number and inertia parameter, but it falls with a higher Prandtl number and magnetic parameter. Table 7 shows the numerical outcome of the HAM solution at dissimilar approximations based on the use of different values of embedding parameters. It is seen from the table that the HAM

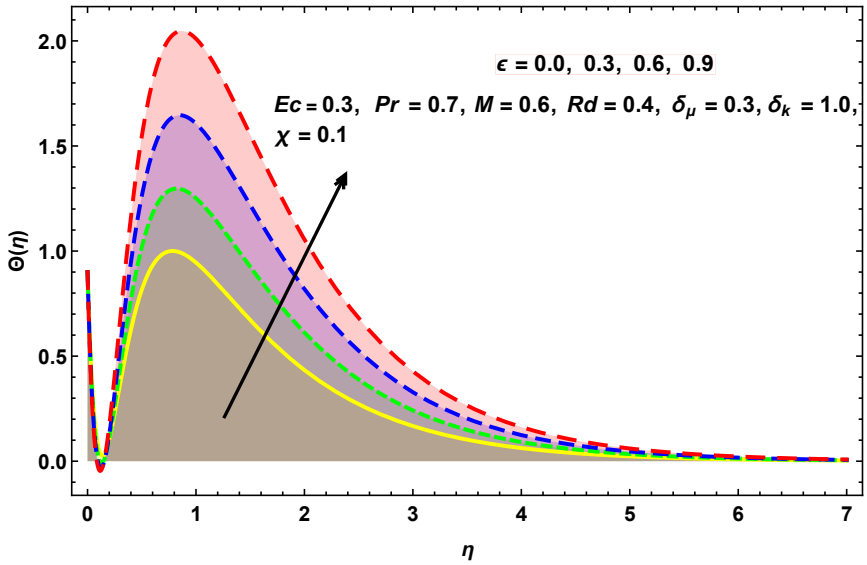

Figure 12. Variations of $\Theta(\eta)$ for several values of ϵ.

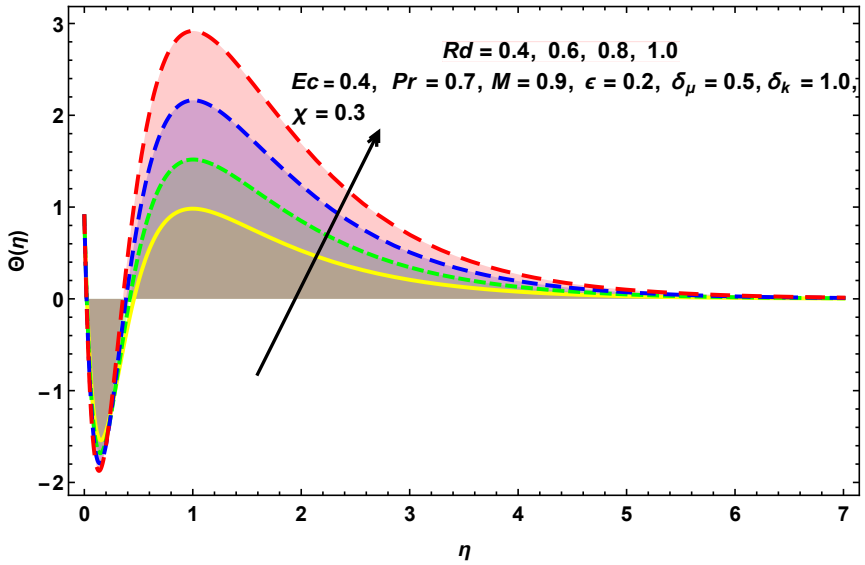

Figure 13. Variations of $\Theta(\eta)$ for several values of Rd.

method is a quickly convergent technique.

Table 3. Comparison with existing literature for $F''(\eta)$ when $\delta_\mu = \delta_k = 0$.

	$F''(\eta)$ when $\epsilon = 0.0$			$F''(\eta)$ when ϵ = -1.0		
χ	Ishak et al. [16]	Qasim et al. [52]	Present	Ishak et al. [16]	Qasim et al. [52]	Present
0.1	1.2888	1.2887	1.2878	3.7162	3.7037	3.7024
0.01	8.4924	8.4912	8.4907	26.6021	26.5994	26.5986
0.001	62.1637	62.1573	62.1492	197.2699	196.8878	196.7682

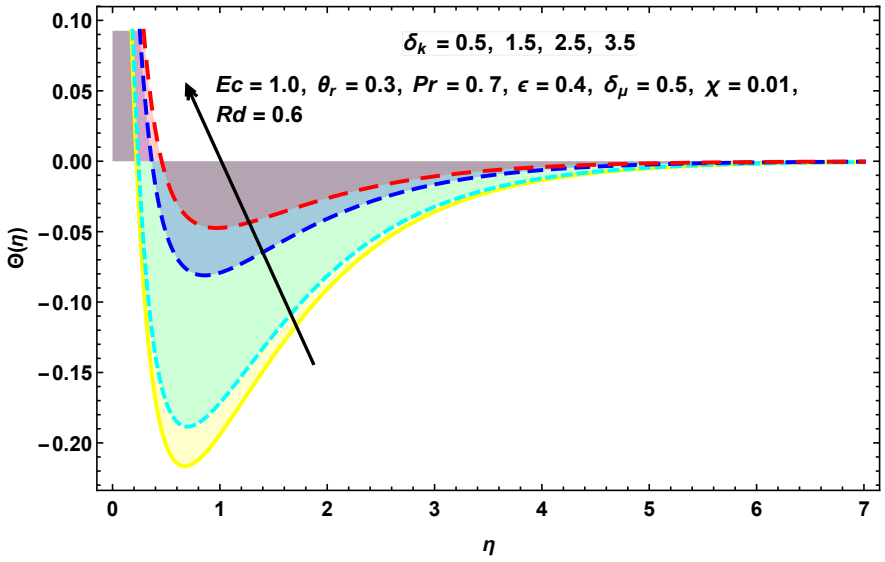

Figure 14. Variations of $\Theta(\eta)$ for several values of δ_k.

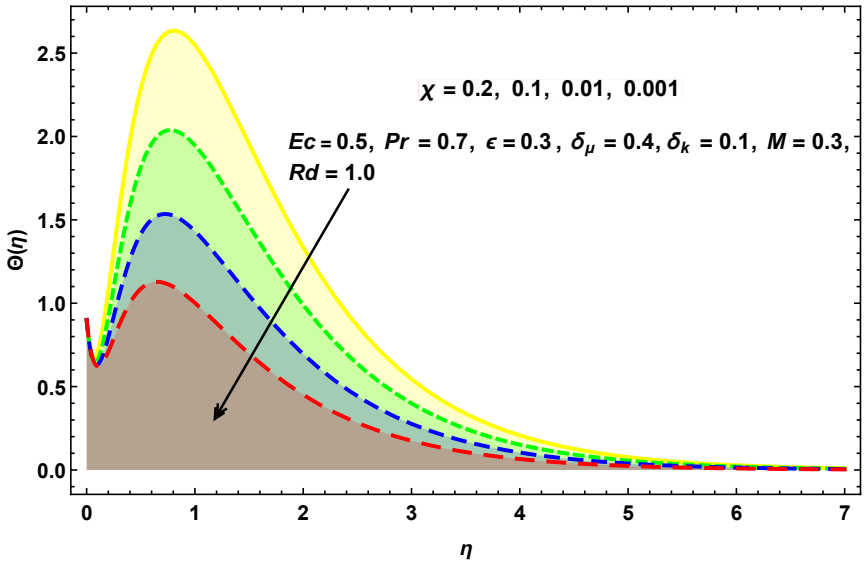

Figure 15. Variations of $\Theta(\eta)$ for several values of χ.

6. Concluding remarks and observations

In the current work, a steady 2D boundary layer MHD nanofluid flow with nonlinear thermal radiation over a horizontally moving thin needle has been analyzed. The needle was inserted horizontally in the nanofluid under certain physical conditions. The governing PDEs have been transformed into a set of ODEs by employing a similarity transformation and solving the equations together with the BCs by using the HAM in Mathematica software. An analytical approach has been carried out for the current flow problem. The influence of several physical factors upon the flow and thermal profiles has been discussed and illustrated by means of graphs. After the detailed analysis of the current study, the following points were identified:

Table 4. Comparison with existing literature for $Re^{\frac{1}{2}}C_f$ and $Re^{-\frac{1}{2}}Nu$.

		$Re^{\frac{1}{2}}C_f$ when $\chi = 0.1$, $\epsilon = 0.4$ and $Ec = 0.5$		$Re^{-\frac{1}{2}}Nu$ when $\chi = 0.1$, $\epsilon = 0.4$ and $Ec = 0.5$	
δ_μ	δ_k	Qasim et al. [52]	Present	Qasim et al. [52]	Present
0.0		0.6549	0.1404	1.7283	0.86083
0.2		0.6003	0.1046	1.7298	0.86088
0.3		0.5882	0.0909	1.7303	0.86090
0.4		0.5601	0.0791	1.7307	0.86092
	0.0	0.5756	0.0910	1.9169	0.92876
	0.2	0.5715	0.0909	1.7503	0.87973
	0.3	0.5803	0.0907	1.6577	0.86090
	0.6	0.5846	0.0905	1.4914	0.81864

Table 5. Impact of $Re^{\frac{1}{2}}C_f$ when $\delta_\mu = 0.3$, $\chi = 0.1$ and $Pr = 0.7$.

ϵ	M	k_1	F_r	$Re^{\frac{1}{2}}C_f$
0.1	0.1	0.3	0.1	0.63731
0.2				0.44124
0.3				0.24427
	0.2			1.09767
	0.4			1.12209
	0.6			1.14718
		1.0		1.21409
		1.5		1.28491
		2.0		1.35999
			0.15	0.91346
			0.20	0.99803
			0.25	1.00037

- When the magnetic effect is applied to a flow system, it produces a Lorentz force that opposes the flow system's velocity which results in decreasing the flow characteristics.
- Decreases in the values of χ results in a reduction of the fluid's temperature and augmentation in the fluid flow.
- The velocity of the nanofluid reduces by enhancing the values of the porosity and variable viscosity parameters.
- The velocity profile trends upwards when the rate of inertia parameter increases.
- With growth in the radiation parameter, the temperature ratio parameter, thermal conductivity parameter, velocity ratio parameter and Eckert number, there is an upsurge in the temperature field.
- The growing value of the Prandtl number reduces the fluid's temperature.
- Skin friction is increased by increasing the magnetic, porosity and inertial parameters, whereas an opposite effect is noticed by varying the velocity ratio parameter.
- The Nusselt number increases by enhancing the inertia parameter and Eckert number, whereas an opposite effect is noticed by varying the Prandtl number and the magnetic parameter.

Table 6. Impact of $Re^{-\frac{1}{2}}Nu$ when $\delta_\mu = 0.3$, $\chi = 0.001$ and $\theta_r = 0.1$.

Pr	Ec	F_r	M	$Re^{-\frac{1}{2}}Nu$
0.7	0.5	0.1	0.4	0.08830
3.0				0.08877
6.3				0.08893
	1.0			0.08196
	1.5			0.07814
	2.0			0.07432
		0.3		0.08961
		0.5		0.08617
		0.7		0.08555
			0.6	0.08585
			0.8	0.08590
			1.0	0.08694

Table 7. Convergence of HAM for n = 0 and n = 1 when δ_μ=δ_k = 0.3 and Pr = 0.7.

	when n = 0		when n = 1	
Order of approximation	$F''(0)$	$\Theta'(0)$	$F''(0)$	$\Theta'(0)$
1	1.46317	1.39317	-0.96027	-0.86937
5	1.43102	1.39246	-0.95318	-0.86415
10	1.42635	1.37157	-0.91240	-0.85360
15	1.42326	1.36295	-0.90635	-0.84415
20	1.42015	1.36054	-0.84163	-0.83061
25	1.40361	1.32001	-0.84125	-0.83005

- Existing results in the literature were compared with those of the present study.
- The tendency of the HAM to converge with the variation in physical parameters was examined numerically.

Acknowledgments

This research was supported by the National Science, Research and Innovation Fund (NSRF), Thailand.

Conflict of interest

The authors declare that there is no conflict of interest.

References

1. L. Prandtl, On fluid motions with very small friction, in *3rd International Congress of Mathematicians*, **3** (1904), 484–491.

2. D. W. Schaefer, Engineered porous materials, *MRS Bull.*, **19** (1994), 14–19. https://doi.org/10.1557/S0883769400039452

3. M. W. Shafer, D. D. Awschalom, J. Warnock, G. Ruben, The chemistry of and physics with porous sol-gel glasses, *J. Appl. Phys.*, **61** (1987), 5438–5446. https://doi.org/10.1063/1.338285

4. S. Bilal, M. Sohail, R. Naz, Heat transport in the convective Casson fluid flow with homogeneous-heterogeneous reactions in Darcy-Forchheimer medium, *Multidiscip. Model. Mater. Struct.*, **15** (2019), 1170–1189. https://doi.org/10.1108/MMMS-11-2018-0202

5. R. Naz, S. Tariq, M. Sohail, Z. Shah, Investigation of entropy generation in stratified MHD Carreau nanofluid with gyrotactic microorganisms under Von Neumann similarity transformations, *Eur. Phys. J. Plus.*, **135** (2020), 1–22. https://doi.org/10.1104/epjp/s13360-019-00069-0

6. R. Naz, F. Mabood, M. Sohail, I. Tlili, Thermal and species transportation of Eyring-Powell material over a rotating disk with swimming microorganisms: applications to metallurgy, *J. Mater. Res. Technol.*, **9** (2020), 5577–5590. https://doi.org/10.1016/j.jmrt.2020.03.082

7. G. Rasool, N. A. Shah, E. R. El-Zahar, A. Wakif, Numerical investigation of EMHD nanofluid flows over a convectively heated riga pattern positioned horizontally in a Darcy-Forchheimer porous medium: Application of passive control strategy and generalized transfer laws, *Waves Random Complex Media*, (2022), 1–20. https://doi.org/10.1080/17455030.2020.2074571

8. S. K. Das, S. U. Choi, W. Yu, T. Pradeep, *Nanofluids: Science and Technology*, John Wiley & Sons, 2007.

9. A. S. Dogonchi, M. Waqas, S. M. Seyyedi, M. Hashemi-Tilehnoee, D. D. Ganji, A modified Fourier approach for analysis of nanofluid heat generation within a semi-circular enclosure subjected to MFD viscosity, *Int. Commun. Heat Mass Transf.*, **111** (2020), 1–9. https://doi.org/10.1016/j.icheatmasstransfer.2019.104430

10. S. S. M. Ajarostaghi, M. A. Delavar, S. Poncet, Thermal mixing, cooling and entropy generation in a micromixer with a porous zone by the lattice Boltzmann method, *J. Therm. Anal. Calorim.*, **140** (2020), 1321–1339. https://doi.org/10.1007/s10973-019-08386-3

11. Z. Abdelmalek, T. Tayebi, A. S. Dogonchi, A. J. Chamkha, D. D. Ganji, I. Tlili, Role of various configurations of a wavy circular heater on convective heat transfer within an enclosure filled with nanofluid, *Int. Commun. Heat Mass Transf.*, **113** (2020), 1–16. https://doi.org/10.1016/j.icheatmasstransfer.2020.104525

12. L. L. Lee, Boundary layer over a thin needle, *Phys. Fluids*, **10** (1967), 820–822. https://doi.org/10.1063/1.1762194

13. J. L. S. Chen, T. N. Smith, Forced convection heat transfer from nonisothermal thin needles, *J. Heat Transf.*, **100** (1978), 358–362. https://doi.org/10.1115/1.3450809

14. T. Grosan, I. Pop, Forced convection boundary layer flow past nonisothermal thin needles in nanofluids, *J. Heat Transf.*, **133** (2011), 1–4. https://doi.org/10.1115/1.4003059

15. C. Y. Wang, Mixed convection on a vertical needle with heated tip, *Phys. Fluids*, **2** (1990), 622–625. https://doi.org/10.1063/1-857709

16. A. Ishak, R. Nazar, I. Pop, Boundary layer flow over a continuously moving thin needle in a parallel free stream, *Chin. Phys. Lett.*, **24** (2007), 2895–2897. https://doi.org/10.1088/0256-307X/24/10/051

17. M. K. Nayak, A. Wakif, I. L. Animasaun, M. Alaoui, Numerical differential quadrature examination of steady mixed convection nanofluid flows over an isothermal thin needle conveying metallic and metallic oxide nanomaterials: a comparative investigation, *Arab. J. Sci. Eng.*, **45** (2020), 5331–5346. https://doi.org/10.1007/s13369-020-04420-x

18. E. A. Algehyne, A. Wakif, G. Rasool, A. Saeed, Z. Ghouli, Significance of Darcy-Forchheimer and Lorentz forces on radiative alumina-water nanofluid flows over a slippery curved geometry under multiple convective constraints: a renovated Buongiorno's model with validated thermophysical correlations, *Waves Random Complex Media*, (2022), 1–30. https://doi.org/10.1080/17455030.2020.2074570

19. T. Hayat, M. I. Khan, M. Farooq, T. Yasmeen, A. Alsaedi, Water-carbon nanofluid flow with variable heat flux by a thin needle, *J. Mol. Liq.*, **224** (2016), 786–791. https://doi.org/10.1016/j.molliq.2016.10.069

20. R. Ahmad, M. Mustafa, S. Hina, Buongiorno model for fluid flow around a moving thin needle in a flowing nanofluid: A numerical study, *Chin. J. Phys.*, **55** (2017), 1264–1274. https://doi.org/10.1016/j.cjph.2017.07.004

21. J. P. Narain, M. S. Uberoi, Combined forced and free-convection heat transfer from vertical thin needles in a uniform stream, *Phys. Fluids*, **15** (1972), 1879–1882. https://doi.org/10.1063/1.1693798

22. S. Ahmad, N. M. Arifin, R. Nazar, I. Pop, Mixed convection boundary layer flow along vertical thin needles: Assisting and opposing flows, *Int. Commun. Heat Mass Transf.*, **35** (2008), 157–162. https://doi.org/10.1016/j.icheatmasstransfer.2007.07.005

23. M. I. Afridi, I. Tlili, M. Qasim, I. Khan, Nonlinear Rosseland thermal radiation and energy dissipation effects on entropy generation in CNTs suspended nanofluids flow over a thin needle, *Bound. Value Probl.*, **2018** (2018), 1–14. https://doi.org/10.1186/s13661-018-1062-3

24. C. Sulochana, S. R. Aparna, N. Sandeep, Impact of linear/nonlinear radiation on incessantly moving thin needle in MHD quiescent Al-Cu/methanol hybrid nanofluid, *Int. J. Ambient Energy*, **43** (2022), 2694–2700. https://doi.org/10.1080/01430750.2020.1768895

25. C. Sulochana, G. P. Ashwinkumar, N. Sandeep, Joule heating effect on a continuously moving thin needle in MHD Sakiadis flow with thermophoresis and Brownian moment, *Eur. Phys. J. Plus.*, **132** (2017), 1–14. https://doi.org/10.1140/epjp/i2017-11633-3

26. S. Nadeem, S. Zaheer, T. Fang, Effects of thermal radiation on the boundary layer flow of a Jeffrey fluid over an exponentially stretching surface, *Numer. Algorithms*, **57** (2011), 187–205. https://doi.org/10.1007/s11075-010-9423-8

27. S. Arulmozhi, K. Sukkiramathi, S. S. Santra, R. Edwan, U. Fernandez-Gamiz, S. Noeiaghdam, Heat and mass transfer analysis of radiative and chemical reactive effects on MHD nanofluid over an infinite moving vertical plate, *Results Eng.*, **14** (2022), 1–9. https://doi.org/10.1016/j.rineng.2022.100394

28. B. Manvi, J. Tawade, M. Biradar, S. Noeiaghdam, U. Fernandez-Gamiz, V. Govindan, The effects of MHD radiating and non-uniform heat source/sink with heating on the momentum and heat transfer of Eyring-Powell fluid over a stretching, *Results Eng.*, **14** (2022), 1–11. https://doi.org/10.1016/j.rineng.2022.100435
29. T. Tayebi, A. S. Dogonchi, N. Karimi, H. Ge-JiLe, A. J. Chamkha, Y. Elmasry, Thermo-economic and entropy generation analyses of magnetic natural convective flow in a nanofluid-filled annular enclosure fitted with fins, *Sustain. Energy Technol. Assess.*, **46** (2021), 1–30. https://doi.org/10.1016/j.seta.2021.101274
30. A. J. Chamkha, A. S. Dogonchi, D. D. Ganji, Magnetohydrodynamic nanofluid natural convection in a cavity under thermal radiation and shape factor of nanoparticles impacts: a numerical study using CVFEM, *Appl. Sci.*, **8** (2018), 1–16. https://doi.org/10.3390/app8122396
31. S. M. Seyyedi, A. S. Dogonchi, M. Hashemi-Tilehnoee, D. D. Ganji, A. J. Chamkha, Second law analysis of magneto-natural convection in a nanofluid filled wavy-hexagonal porous enclosure, *Int. J. Numer. Methods Heat Fluid Flow*, **30** (2020), 4811–4836. https://doi.org/10.1108/HFF-11-2019-0845
32. A. S. Dogonchi, M. Waqas, S. R. Afshar, S. M. Seyyedi, M. Hashemi-Tilehnoee, A. J. Chamkha, et al., Investigation of magneto-hydrodynamic fluid squeezed between two parallel disks by considering Joule heating, thermal radiation, and adding different nanoparticles, *Int. J. Numer. Methods Heat Fluid Flow*, **30** (2019), 659–680. https://doi.org/10.1108/HFF-05-2019-0390
33. A. Wakif, A novel numerical procedure for simulating steady MHD convective flows of radiative Casson fluids over a horizontal stretching sheet with irregular geometry under the combined influence of temperature-dependent viscosity and thermal conductivity, *Math. Probl. Eng.*, **2020** (2020), 1–20. https://doi.org/10.1155/2020/1675350
34. N. Sandeep, B. Ranjana, S. P. Samrat, G. P. Ashwinkumar, Impact of nonlinear radiation on magnetohydrodynamic flow of hybrid nanofluid with heat source effect, *Proc. Inst. Mech. Eng. E: J. Process Mech. Eng.*, **236** (2022), 1616–1627. https://doi.org/10.1177/09544089211070667
35. S. N. A. Salleh, N. Bachok, N. M. Arifin, F. M. Ali, I. Pop, Magnetohydrodynamics flow past a moving vertical thin needle in a nanofluid with stability analysis, *Energies*, **11** (2018), 1–15. https://doi.org/10.3390/en11123297
36. P. M. Krishna, R. P. Sharma, N. Sandeep, Boundary layer analysis of persistent moving horizontal needle in Blasius and Sakiadis magnetohydrodynamic radiative nanofluid flows, *Nucl. Eng. Technol.*, **49** (2017), 1654–1659. https://doi.org/10.1016/j.net.2017.07.023
37. Z. Khan, M. Jawad, E. Bonyah, N. Khan, R. Jan, Magnetohydrodynamic thin film flow through a porous stretching sheet with the impact of thermal radiation and viscous dissipation, *Math. Probl. Eng.*, **2022** (2022), 1–10. https://doi.org/10.1155/2022/1086847
38. M. Jawad, Z. Khan, E. Bonyah, R. Jan, Analysis of hybrid nanofluid stagnation point flow over a stretching surface with melting heat transfer, *Math. Probl. Eng.*, **2022** (2022), 1–12. https://doi.org/10.1155/2022/9469164
39. M. Ramzan, H. Gul, S. Kadry, C. Lim, Y. Nam, F. Howari, Impact of nonlinear chemical reaction and melting heat transfer on an MHD nanofluid flow over a thin needle in porous media, *Appl. Sci.*, **9** (2019), 1–14. https://doi.org/10.3390/app9245492

40. H. Upreti, M. Kumar, Influence of non-linear radiation, Joule heating and viscous dissipation on the boundary layer flow of MHD nanofluid flow over a thin moving needle, *Multidiscip. Model. Mater. Struct.*, **16** (2019), 208–224. https://doi.org/10.1108/MMMS-05-2019-0097

41. C. Sulochana, G. P. Ashwinkumar, N. Sandeep, Boundary layer analysis of persistent moving horizontal needle in magnetohydrodynamic ferrofluid: A numerical study, *Alex. Eng. J.*, **57** (2018), 2559–2566. https://doi.org/10.1016/j.aej.2017.08.020

42. A. Hamid, Terrific effects of Ohmic-viscous dissipation on Casson nanofluid flow over a vertical thin needle: buoyancy assisting & opposing flow, *J. Mater. Res. Technol.*, **9** (2020), 11220–11230. https://doi.org/10.1016/j.jmrt.2020.07.070

43. S. S. Raju, K. G. Kumar, M. Rahimi-Gorji, I. Khan, Darcy-Forchheimer flow and heat transfer augmentation of a viscoelastic fluid over an incessant moving needle in the presence of viscous dissipation, *Microsyst. Technol.*, **25** (2019), 3399–3405. https://doi.org/10.1007/s00542-019-04340-3

44. U. Farooq, M. I. Afridi, M. Qasim, D. Lu, Transpiration and viscous dissipation effects on entropy generation in hybrid nanofluid flow over a nonlinear radially stretching disk, *Entropy*, **20** (2018), 1–14. https://doi.org/10.3390/e20090668

45. T. Nazar, M. M. Bhatti, E. E. Michaelides, Hybrid (Au-TiO2) nanofluid flow over a thin needle with magnetic field and thermal radiation: Dual solutions and stability analysis, *Microfluid. Nanofluid.*, **26** (2022), 1–12. https://doi.org/10.1007/s10404-021-02504-0

46. A. T. Akinshilo, F. Mabood, A. O. Ilegbusi, Heat generation and nonlinear radiation effects on MHD Casson nanofluids over a thin needle embedded in porous medium, *Int. Commun. Heat Mass Transf.*, **127** (2011), 1–13. https://doi.org/10.1016/j.icheatmasstransfer.2021.105547

47. L. Noeiaghdam, S. Noeiaghdam, D. Sidorov, Dynamical control on the homotopy analysis method for solving nonlinear shallow water wave equation, *J. Phys. Conf. Ser.*, **1847** (2021), 1–11. https://doi.org/10.1088/1742-6596/1847/1/012010

48. S. Noeiaghdam, M. A. F. Araghi, S. Abbasbandy, Finding optimal convergence control parameter in the homotopy analysis method to solve integral equations based on the stochastic arithmetic, *Numer. Algorithms*, **81** (2019), 237–267. https://doi.org/10.1007/s11075-018-0546-7

49. S. Noeiaghdam, E. Zarei, H. B. Kelishami, Homotopy analysis transform method for solving Abel's integral equations of the first kind, *Ain Shams Eng. J.*, **7** (2016), 483–495. https://doi.org/10.1016/j.asej.2015.03.006

50. S. Noeiaghdam, M. A. F. Araghi, A novel approach to find optimal parameter in the homotopy-regularization method for solving integral equations, *Appl. Math. Inf. Sci.*, **14** (2020), 99–107. https://dx.doi.org/10.18576/amis/140114

51. A. D. Fragkou, T. E. Karakasidis, I. E. Sarris, Recurrence quantification analysis of MHD turbulent channel flow, *Phys A: Stat. Mech. Appl.*, **531** (2019), 1–14. https://doi.org/10.1016/j.physa.2019.121741

52. M. Qasim, N. Riaz, D. Lu, M. I. Afridi, Flow over a needle mving in a stream of dissipative fluid having variable viscosity and thermal conductivity, *Arab. J. Sci. Eng.*, **46** (2021), 7295–7302. https://doi.org/10.1007/s13369-021-05352-w

53. I. Tlili, M. Ramzan, S. Kadry, H. W. Kim, Y. Nam, Radiative MHD nanofluid flow over a moving thin needle with entropy generation in a porous medium with dust particles and Hall current, *Entropy*, **22** (2020), 1–17. https://doi.org/10.3390/e22030354

54. O. D. Makinde, Entropy-generation analysis for variable-viscosity channel flow with non-uniform wall temperature, *Appl. Energy*, **85** (2008), 384–393. https://doi.org/10.1016/j.apenergy.2007.07.008

55. A. Khan, W. Kumam, I. Khan, A. Saeed, T. Gul, P. Kumam et al., Chemically reactive nanofluid flow past a thin moving needle with viscous dissipation, magnetic effects and hall current, *Plos One*, **16** (2021), 1–18. https://doi.org/10.1371/journal.pone.0249264

56. M. Bilal, Y. Urva, Analysis of non-Newtonian fluid flow over fine rotating thin needle for variable viscosity and activation energy, *Arch. Appl. Mech.*, **91** (2021), 1079–1095. https://doi.org/10.1007/s00419-020-01811-2

57. J. R. Reddy, V. Sugunamma, N. Sandeep, C. Sulochana, Influence of chemical reaction, radiation and rotation on MHD nanofluid flow past a permeable flat plate in porous medium, *J. Niger. Math.*, **35** (2016), 48–65. https://doi.org/10.1016/j.jnnms.2015.08.004

58. S L., *The Proposed Homotopy Analysis Technique for the Solution of Nonlinear Problems*, Doctoral dissertation, PhD thesis, Shanghai Jiao Tong University, 1992.

59. M. Hatami, R. Nouri, D. D. Ganji, Forced convection analysis for MHD Al2O3–water nanofluid flow over a horizontal plate, *J. Mol. Liq.*, **187** (2013), 294–301. https://doi.org/10.1016/j.molliq.2013.08.008

AIMS Press